ORIGINAL PAPER

Response Characteristics of Slope Subjected to Blasting: A Case Study in Manaoke Open-pit Gold Mine

Qinglin Li · Bijiang Dai · Lujun Long · Dongming Zhang · **Feng Liang**

Abstract Frequent production blasting is an important factor affecting the slope stability in open-pit mines; thus, it is essential to monitor and analyze blasting vibrations in open-pit mines. In this study, blasting vibration on the slope of an open-pit gold mine in Manaoke was monitored. First, regression analysis was performed on the monitoring results using the Sadowski formula, and the attenuation law of the slope blasting vibration was established. Second, the damage depth of the retained rock mass was determined using ultrasonic velocimetry, and the relationship between the damage depth and peak particle vibration velocity was fitted. Third, the Midas numerical software was used to analyze the stability of the slope under blasting vibration conditions. The results showed that the fitted vibration attenuation formula was close for four consecutive days, and the slope blasting activity was within a safe range. Ultrasonic velocity measurements showed that the damage depth of the reserved rock mass after blasting was between 1.0 and 1.5 m. The damage depth had a good correlation with the peak particle vibration velocity, which can adequately predict future reserved rock mass damage. The final numerical calculation results showed that the slope was in a stable state, and the slope stability was not considerably affected under the daily blasting vibration conditions. Thus, the blasting activities were in a safe range.

Keywords Production blasting · Vibration attenuation law · Damage depth · Slope stability · Numerical simulation

Q. Li · D. Zhang (✉)
State Key Laboratory of Coal Mine Disaster Dynamicsand Control, Chongqing University, Chongqing 400044, China
e-mail: zhangdm@cqu.edu.cn

Q. Li · D. Zhang
School of Resources and Safety Engineering, Chongqing University, Chongqing 400044, China

B. Dai · L. Long
Chongqing Geological Group, Manaoke Gold Mine Company, Chongqing, China

F. Liang
No 208 Hydrogeology and Engineering Geology Team, Chongqing Bureau of Geology and Minerals Exploration, Chongqing, China

1 Introduction

Rapid economic development is increasing demand for mineral resources, which are obtained through mining. Compared with underground mining, open-pit mining is more efficient and has a larger scale and freer in operating space. However, continuous mining activities gradually expand the scale of open-pit mine slopes; moreover, frequent blasting damages the rock mass, forming an excavation damage area. The damage area further expands when exposed to adverse conditions, such as subsequent excavation activities and rainfall, which consequently affect slope stability.

Therefore, it is necessary to monitor and control the blasting process, determine the scope of the damage area in real time, and evaluate the blasting influence on slope stability. These steps will help to establish corresponding measures for reducing the harm caused by the blasting process.

Several studies have been conducted on reducing the influence of blasting excavation on slope stability. He et al. (2013) conducted a comparative test and found that pre-cracks can absorb most of the blasting vibration energy; hence, the authors reported that pre-crack blasting can improve the safety and stability of open-pit mine slopes. Xie et al. (2018) monitored blasting vibration data and used the lS-DYNA software to back analyze the data and simulate six different blasting methods. Consequently, the authors proposed a more appropriate blasting method. Man et al. (2021) designed smooth blasting parameters and corresponding blasting vibration monitoring schemes for the high-level radioactive waste geological disposal project of BET. Blasting vibration is mainly monitored using a blasting vibration tester, and the most commonly used tester is TC-6850. Zhu et al. (2019) designed an automatic monitoring system of blasting vibration based on the TC-6850 vibration tester to improve monitoring efficiency. Monitoring the blasting vibration process provides sufficient data to analyze the seismic wave attenuation formula under such geological conditions; the formula can also be used to determine the relationship between rock damage depth and peak particle vibration velocity, providing a more convenient approach to predict rock damage. Song et al. (2000) proposed an empirical formula for predicting slope damage by calculating and analyzing the blasting vibration data of an open-pit mine slope. The formula incorporates the vertical particle vibration velocity based on the concept of the vibration strength evaluation method. Yan. (2007) obtained the relationship between cumulative damage and number of blasts by analyzing the results of RSM-SY5 intelligent sound wave apparatus and those of the blasting vibration tester. On the other hand, the study of slope stability in addition to the calculation, field monitoring and analysis from the aspects of mechanical damage depth, can also adopt numerical simulation, and there is enough excellent function to calculation the stability of slope in Midas, UDEC, Abaqus FEA, and Flac-3D. Lu et al. (2012) simulated failure patterns and deformation processes using UDEC through three-dimensional (3D) and two-dimensional (2D) discrete element methods, respectively. Furthermore, Shen et al. (2012) developed a program for transforming geographic information system (GIS) data into a commercial finite difference code (FLAC) by using FLAC's built-in programming language. To demonstrate the reliability of this technique, the authors performed stability analysis of Xuecheng slope in 2D and 3D. The approach of using a GIS software for preprocessing data for numerical slope simulation saves time and money while providing real-world data for numerical modeling applications.

The slope of the Manaoke open-pit gold mine was examined in this study. A blasting vibrometer was used to monitor the blasting, and the Sadowski formula was used to perform the regression analysis of the monitoring results to obtain the vibration attenuation law. Subsequently, the damage depth of the reserved rock mass after blasting was measured and analyzed using a rock ultrasonic velocimeter. The damage depth—peak particle vibration velocity curve was fitted. Finally, the Midas numerical software was used to determine the slope stability under blasting vibration conditions. The stability of the Manaoke open-pit gold mine under blasting conditions was evaluated from multiple perspectives by combining the field monitoring data with the numerical simulation results. The novelty of this study is outlined as follows:

1. The relationship between particle vibration velocity and damage depth of rock mass is established through theoretical analysis of in-situ monitoring data, which can greatly reduce the workload of acoustic detection of large area damaged slope.
2. Previous studies mainly used a 2D profile for the numerical simulation model of slope stability. Here, unmanned aerial vehicle (UAV) technology was used to obtain the actual slope terrain through real-time scanning; the actual terrain was introduced into the Midas software to establish a 1:1 3D model. This method considerably improved the accuracy of the model.
3. Previous studies mainly used the results of the indoor mechanical properties test of rock as the rock stratum parameters, ignoring the influence of the structural plane of rock mass and other field conditions. In this study, the strength of the indoor mechanical test was reduced by combin-

ing the test results of a borehole television camera with a geological strength index (GSI) criterion. This approach was used to obtain more accurate rock stratum parameters and improve the accuracy of the calculation results.

4. In previous studies, slope stability was mainly studied under the condition of static load and certain intensity of seismic wave. In this paper, the actual waveform recorded in the field is input into Midas to simulate the slope stability in the blasting process, and the calculated results are compared with the actual situation, which is highly restored to the actual blasting process in the field.

2 Project Overview

The Jiuzhaigou Manaoke open-pit gold mine in Sichuan Province is in the northwest of Sichuan Plateau and intersects the southern side of Gansu Province, which is a plateau. The mining area extends from Yangbuliangzi in the north to Dongguashubagou in the south (north high slope terrain) and from Yangbulianggou in the west to Luerjiugou in the east (south low slope terrain). The geographical location is shown in Fig. 1. The mining area adopts the phased

mining plan (that is, beginning with opencast and translating to underground mining).

2.1 Engineering Geology Overview

By combining the structural characteristics of rock mass with rock firmness and weathering degree, the outcrop strata can be categorized into loose accumulation, soft, semi-hard, and hard rock groups. The semi-hard and hard rock groups account for a higher proportion of the categories. The semi-hard rock formation is composed of the T_2zg^1 and T_2zg^2 strata; the lithology is composed of thin-bedded calcareous silty silk cloud slates and metamorphic quartz fine sandstone with limestone lens; the rock mass ranges from broken to relatively broken with well-developed joints and moderate to strong weathering. The hard rock components are distributed in T_2zg^3, all strata toward the north, and the T_3z strata at the southern end of the mine. The lithology is composed of thin- to medium-thickness bedded metamorphic quartz sandstone, greywacke, and microcrystalline limestone. The rock mass is relatively intact with well-developed joints and moderate to breezy weathering. The average compressive strength of indoor rock physical and mechanical tests was 108.7 MPa.
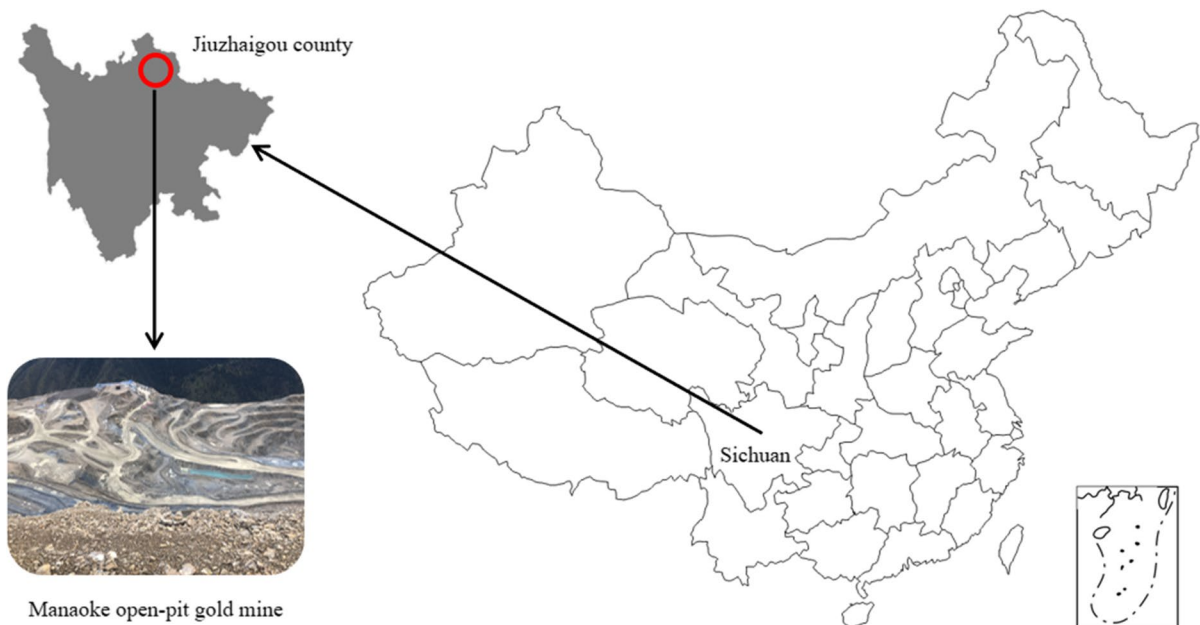

Fig. 1 Geographical location of the slope of Manaoke open-pit gold mine

2.2 Basic Slope Conditions

The highest elevation of the slope is 3550 m, the lowest elevation is 3290 m, the slope height is 260 m, and the final slope angle is 44.47°. The mining production was mainly on the 3290 m platform. The slope structure is complex, where faults, ruffles, joints, and fissures are more developed. The slope contour is shown in Fig. 2.

2.3 Production Blasting Scheme

(1) *Perforation operation*: On the basis of production scale, ore body shape, mining terrain, geological conditions, and ore characteristics, a KG920B drilling machine was used for the perforation operation, as shown in Fig. 3 b. After calculation, three KG920B drilling machines were required; three corresponding LGCY-15/13 air compressors were also required to supply air to the drilling machines. The blast holes were perpendicular to the ground and had a diameter of 100 mm, hole depth of 11.55 m, minimum resistance line of 3.0 m, hole spacing of 4.5 m, and row spacing of 3.9 m. Twelve holes were drilled daily, as shown in

Fig. 3 c. The quincunx hole was adopted to achieve a uniform explosive energy distribution. The layout of the blast hole is shown in Fig. 3 a.

(2) *Blasting operations*: A multi-row, medium-deep hole micro-differential blasting process was adopted on the basis of the mine production scale and the height of production platform. An emulsified explosive and a detonating tube electronic detonator were used to initiate detonation; the emulsion explosive is shown in Fig. 3 d. The single hole charge was 73.5 kg, and the total charge per blast was 882 kg (73.5 kg × 12). The blasting cycle was designed for 20 days, and 12 holes were detonated simultaneously at 6:00 PM each day. The blasting safety distance was 300 m. The blasting material consumption are presented in Table 1.

3 Study on Blasting Vibration Monitoring and Attenuation Law

3.1 Blasting Vibration Monitoring

Currently, a blasting vibration meter is mainly used for the real-time monitoring of production blasting activities in open-pit mining. In this work, the
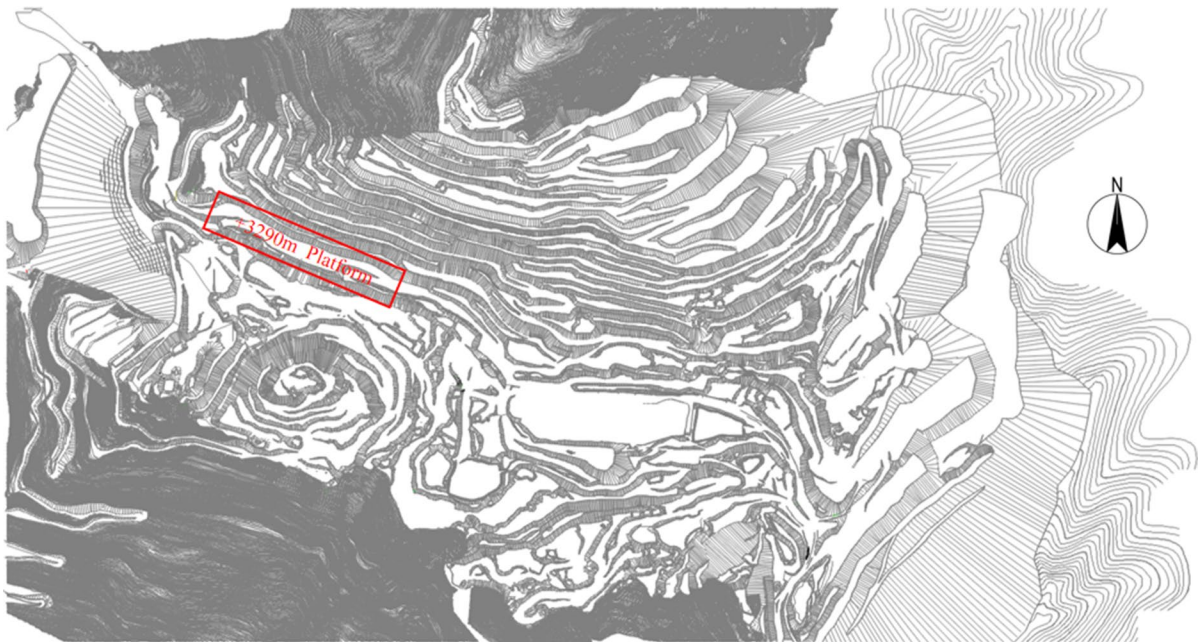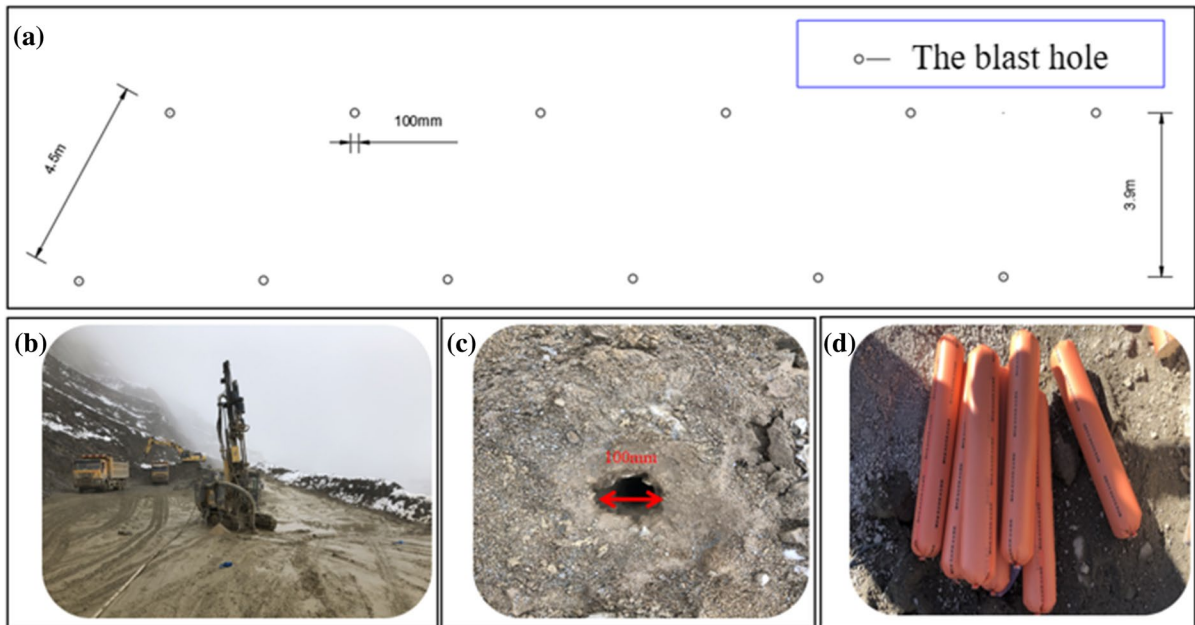

Fig. 2 Contour of the slope

Fig. 3 Blast hole design: **a** Layout of the blast hole; **b** KG920B drilling machine; **c** Blast hole; **d** Emulsion explosive

Table 1 Consumption of blasting materials

Material	Unit	Specific consumption	Mine	Rock	Total
Amount of blasting operation	$10^4 m^3/a$	/	19.8	391.3	411.1
Emulsion explosive	kg	0.25 kg/m^3(mine)	59,288.5	978,260.9	1,037,549.4
		0.3 kg/m^3(rock)			
Non-electric differential detonator	pcs	0.02pcs/m^3	3952.6	78,260.9	82,213.4
Detonating fuse	m	0.001 m/m^3	197.6	3913.0	4110.7
Detonating tube	m	0.12 m/m^3	23,715.4	469,565.2	493,280.6

TC-4850-type blasting vibration tester (Chengdu Zhongke Measurement and Control Company Limited, was used to detect blasting vibration (Zhu et al. 2019). The tester comprises two parts: the main engine and three-axial vibration velocity sensor. The three-axial vibration velocity sensor can record particle vibration velocity in horizontal tangential, horizontal radial, and vertical directions. Before blasting, three blasting vibration testers were positioned at a straight distance of 50 m (monitoring point A), 60 m (monitoring point B), and 70 m (monitoring point C) behind the hole; the three points were on the same platform, as shown in Fig. 4 a. The sensor was glued to the surface using plaster (Nateghi 2012), as shown in Fig. 4 b.

Here, the blasting activities on October 22 (D1), 23 (D2), 24 (D3), and 25 (D4) were monitored for four consecutive days. The blasting vibration monitoring results on the fourth day are shown in Fig. 5.

For each monitoring point, particle vibration velocity curves in three directions were plotted. The test results of these four days showed that the amplitude of particle vibration velocity in the horizontal radial direction was the largest. The peak particle vibration velocity in the horizontal radial direction was 6.56 cm/s at monitoring point A, 5.31 cm/s at monitoring point B, and 3.89 cm/s at monitoring point C. Therefore, the attenuation law of the particle horizontal radial vibration was prioritized (Mesec et al. 2010).
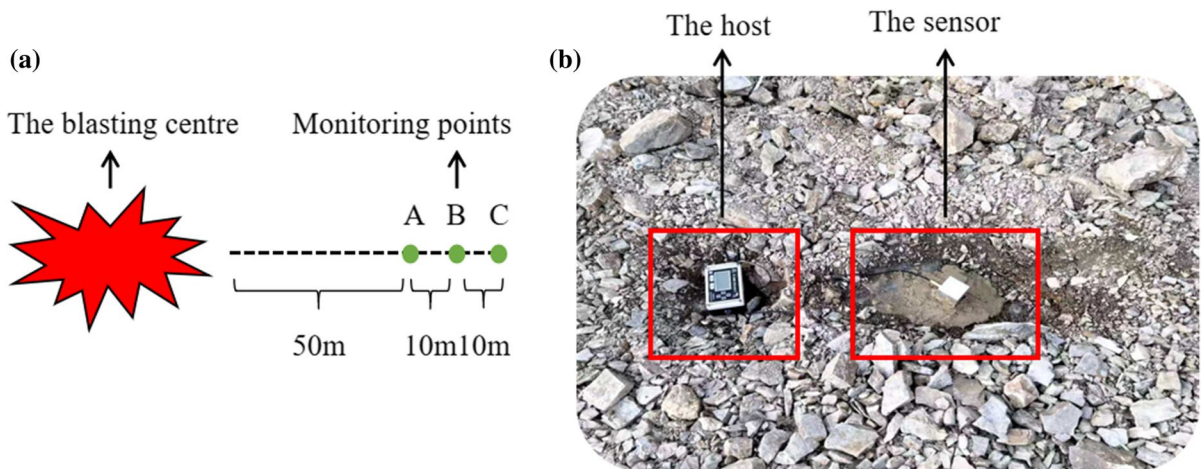
(a)

(b)

Fig. 4 Design of the blasting vibration monitoring: **a** Position of monitoring points; **b** Layout of sensor
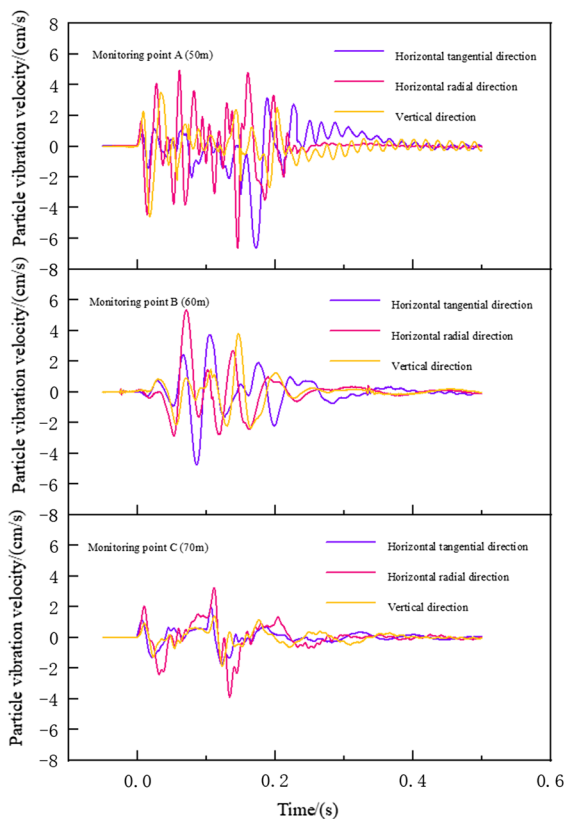

Fig. 5 Blasting vibration test results of D4

3.2 Attenuation Law of Blasting Vibration

The daily explosive quantity in sound and the horizontal radial peak vibration velocity of the measuring point were calculated. The results are shown in Table 2.

To fit the attenuation law of the blasting vibration under the site conditions (Rao and Cai 2016), the date in Table 2 are combined with the Sadowski formula:

$$v = K\rho^\alpha = K\left(\frac{Q^{1/3}}{R}\right)^\alpha \tag{1}$$

where v (cm/s) is the peak particle vibration velocity; ρ(kg$^{1/3}$/m) is the proportional dosage; K is the site coefficient; α is the attenuation coefficient, and K and α are related to the actual geological conditions, blasting method, and charging structure; Q (kg) is the single blasting volume; and R (m) is the blasting center distance. Equation (1) is transformed through regression analysis, and the logarithm of both sides is taken:

$$\lg v = \lg(K\rho^\alpha) = \lg K + \alpha \lg \rho \tag{2}$$

where $y = \lg v$, $b = \lg K$, and $x = \lg \rho$; then:

$$y = \alpha x + b \tag{3}$$

The least square estimation method is used to obtain the values of α and b in Eq. (3):

$$\alpha = \frac{\sum_{i=1}^{3}(xi - \bar{x})yi}{\sum_{i=1}^{3}(xi - \bar{x})^2} \tag{4}$$

Table 2 Statistical results of horizontal radial peak vibration velocity

Date	Single blasting volume/(kg)	/	Blasting center distance/(m)		
			50	60	70
D1	882	Peak particle vibration velocity/(cm/s)	6.31	5.10	3.67
D2			6.37	5.18	3.73
D3			6.15	4.93	3.46
D4			6.56	5.31	3.89

$$b = \bar{y} - \alpha\bar{x} \tag{5}$$

To evaluate the regression effect, a correlation coefficient R is introduced for the significance test:

$$R = \frac{\sum_{i=1}^{3}\left(xi - \bar{x}\right)\left(yi - \bar{y}\right)}{\sqrt{\sum_{i=1}^{3}\left(xi - \bar{x}\right)^2 \sum_{i=1}^{3}\left(yi - \bar{y}\right)^2}} \tag{6}$$

$|R|$ ranges from 0–1; the closer it is to 1, the stronger the linear relationship between x and y in the equation. When $|R|$ exceeds 0.8, the regression analysis is considered reliable; otherwise, the regression analysis should be performed after discarding the larger deviation from the measurement points (Peng et al. 2016). α, K, and $|R|$ on the measurement day can be solved using Eqs. (4), (5), and (6) to obtain the attenuation equation of the horizontal radial vibration under site and blasting conditions, as illustrated in Table 3.

It can be observed from the calculation results that the site coefficient K and attenuation coefficient α were relatively close ($K \in [83.18, 104.71], \alpha \in [1.54, 1.70]$). The closeness was because the geological conditions, blasting methods, and charging structures in the four consecutive days were similar. Additionally, $K \in [50, 350]$, $\alpha \in [1.3, 2.0]$, and $|R| > 0.8$, suggesting that the fitting results were reliable and effective (Wang et al. 2020). Currently, no unified regulation exists on the vibration speed safety range of slope blasting in open-pit mines; however, the data provided by some research institutions show that the safety range of vibration velocity at the foot of a stable slope is 35–42 cm/s, a relatively stable slope is 28–35 cm/s, and a less stable slope is 22–30 cm/s. The monitoring results presented in Table 2 and the calculation results presented in Table 3 show that the production blasting activities of the slope were within the safety range (Ak and Konuk 2008; Aloui and Abbes 2019).

Table 3 Calculation results of attenuation law of horizontal radial vibration

Date	α	b	K	$|R|$	Attenuation formula of horizontal radial vibration
D1	1.60	1.96	91.20	0.9845	$v = 91.20\left(\frac{Q^{1/3}}{R}\right)^{1.60}$
D2	1.58	1.95	89.12	0.9827	$v = 89.12\left(\frac{Q^{1/3}}{R}\right)^{1.58}$
D3	1.70	2.02	104.71	0.9833	$v = 104.71\left(\frac{Q^{1/3}}{R}\right)^{1.70}$
D4	1.54	1.92	83.18	0.9194	$v = 83.18\left(\frac{Q^{1/3}}{R}\right)^{1.54}$

4 Determination of Blasting Damage Depth

In this paper, the damage depth of retained rock is determined by measuring ultrasonic wave velocity of rock mass.

4.1 Quantitative Standard of Blasting Damage Depth

The rock integrity was determined by measuring the ultrasonic velocity before blasting. Subsequently, the ultrasonic velocity was measured on the reserved rock after blasting to determine the depth of blasting damage; the specific quantitative standard is as follows:

$$\eta = \frac{Vp1 - Vp2}{Vp1} \tag{7}$$

where V_{P1} and V_{p2} are the longitudinal wave velocities (km/s) measured before and after rock blasting, respectively; η represents the longitudinal wave velocity decline rate of the rock mass before and after blasting. Currently, the rock mass damage criterion is mainly used in the industry when η reaches 10%; the corresponding rock mass depth is the impact depth of

the production blasting activity on the reserved rock mass (Roy and Sarkar 2017).

4.2 Ultrasonic Velocity Measurement Scheme for Rock Mass

The ultrasonic velocity of the rock mass was measured using a non-metallic ultrasonic detector (JL-IUA6 (A), Wuhan Hualihin Company, China). The main frequency of the instrument was 500 Hz, with an interval of 0.1–200 μs. The recording length was 0.5–1 K, transmission gain was 92 dB, and frequency band width was 100–1000 Hz. A photograph of the instrument is shown in Fig. 6 a.

The double-hole method was adopted for the ultrasonic velocity measurement, and two holes were drilled at the measurement point to explore the sonic emitter and receiver. To measure the initial longitudinal wave velocity of the rock mass before blasting, the sonic holes were drilled before the blasting hole; to measure the longitudinal wave velocity of the reserved rock mass after blasting and reach the reserved rock mass, the depth of acoustic hole exceeded the blasting hole. The depth of the sonic hole was 2 m greater than that of the blasting hole; aperture was 90 mm, and distance between the two

holes was 1 m. The distribution is illustrated in Fig. 6 b.

For four consecutive days, the acoustic velocity of the rock mass was measured before and after blasting. In measuring the velocity, the emitter and receiver were placed at the bottom of the sonic hole at the same time, and water was added as a coupling agent. From the bottom, the transmitter and receiver were continually raised toward the hole at the same time, and the velocity was measured at an interval of 0.1 m, as shown in Fig. 6 c. After the first velocity measurement before blasting each day, the ultra-deep 2-m part at the bottom of the acoustic hole was filled and protected. After blasting, the filling material was cleared before the second velocity measurement.

4.3 Acoustic Test Results

The test results for the four consecutive days are shown in Fig. 7.

As observed from the figure, the reserved rock mass was damaged to varying degrees after daily blasting. The damage depth of the rock mass after daily blasting was determined using Eq. (6); the results are shown in Table 4.
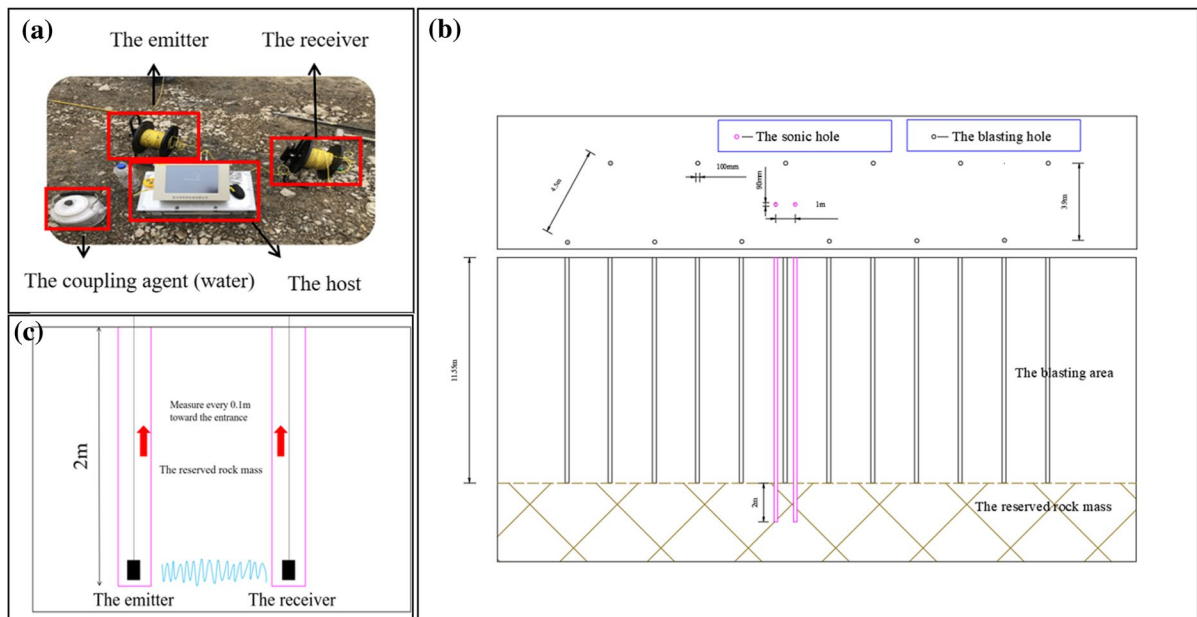

Fig. 6 Ultrasonic velocimetry scheme: **a** Equipment; **b** Distribution of sonic hole; **c** Measurement method

The blasting influence depth ranged from 1.0–1.5 m as the blasting parameters and geological conditions of the blasting site changed slightly in the four consecutive days of the production blasting.

5 Damage Prediction

The damage depth of reserved rock mass increases exponentially with an increase in peak particle vibration velocity (Wei et al. 2009); this relationship can be expressed by Eq. (8):

$$v = Ce^{kh} \tag{8}$$

where C and k are fitting coefficients and h is the damage depth of the reserved rock mass.

Table 4 Damage depth determination results

Date	Depth range of η > 0.1	Depth range of η < 0.1	Depth of blasting damage/ (m)
D1	h1 ≤ 1.2	h2 ≥ 1.3	1.2 ~ 1.3
D2	h1 ≤ 1.2	h2 ≥ 1.3	1.2 ~ 1.3
D3	h1 ≤ 1.0	h1 ≥ 1.1	1.0 ~ 1.1
D4	h1 ≤ 1.4	h2 ≥ 1.5	1.4 ~ 1.5

The logarithm of both sides of Eq. (8) can be obtained as follows:

$$\ln v = kh + \ln C \tag{9}$$

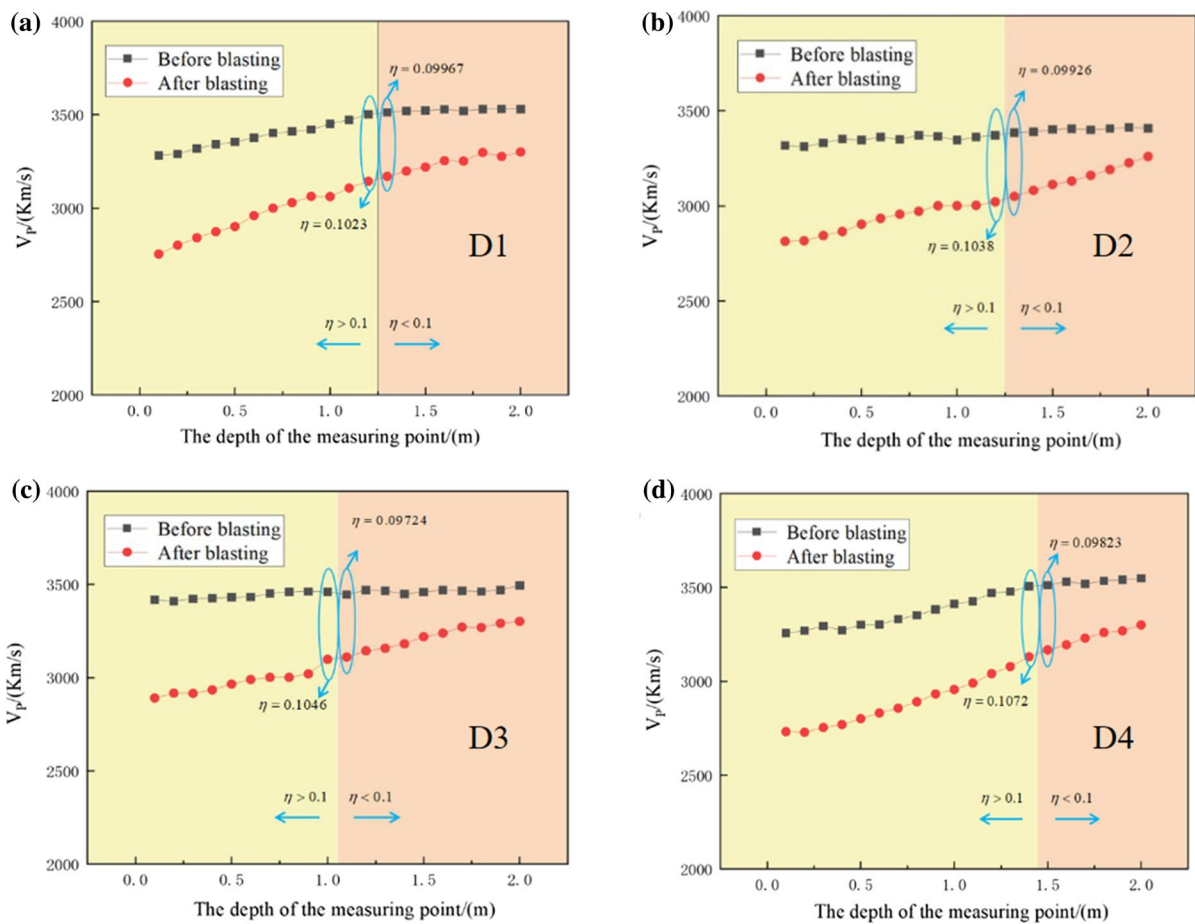Make $y = \ln v$, $x = h$, $b = \ln C$; then

Fig. 7 Wave velocity results of retained rock mass before and after blasting for four consecutive days

$$y = kx + b \qquad (10)$$

Least square estimation was used to obtain the values of k and b and further determine C from the aforementioned data of the peak particle vibration velocity and the damage depth of retained rock mass.

Statistical analyses were conducted on the blasting vibration monitoring data and the corresponding damage depth; the results are shown in Table 5.

We fitted the relationship between the damage depth of the reserved rock mass and the peak particle vibration velocity of particles at different distances from the blasting center distance; the fitting was performed using Eq. (10) and the results presented in Table 5, as shown in Fig. 8.

In subsequent slope blasting activities, the peak particle vibration velocity of the measured point can be used to predict the damage depth of the reserved rock mass at the center of the explosion through the fitting results in Fig. 8. This prediction can serve as a real-time reference for slope support construction.

6 Numerical Analysis of Stability Under Blasting Vibration Condition

In this study, Midas GTS NX was used to numerically determine the blasting vibration condition of the horsehead slope (Niu et al. 2018).

Table 5 Peak particle vibration velocity and corresponding damage depth

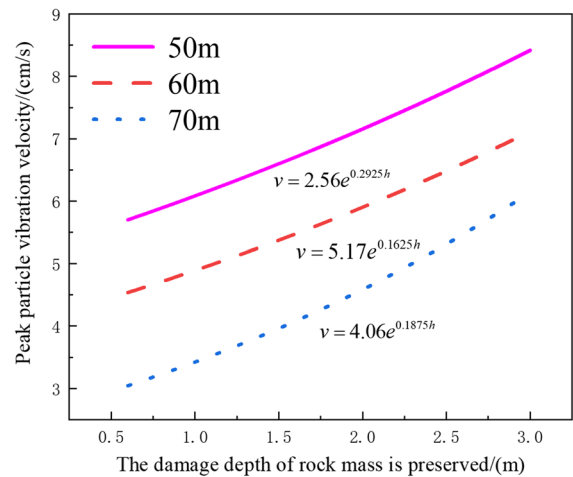| Distance/(m)	Peak particle vibration velocity/(cm/s)	Retaining damage depth of rock mass/ (m)
50	6.31	1.25
	6.37	1.25
	6.15	1.05
	6.56	1.45
60	5.10	1.25
	5.18	1.25
	4.93	1.05
	5.31	1.45
70	3.67	1.25
	3.73	1.25
	3.46	1.05
	3.89	1.45

Fig. 8 Relationship between damage depth of reserved rock mass at different blasting center distances and peak particle vibration velocities

6.1 Model Establishment and Strata Division

UAV technology was used in this modeling process. First, the rough range of the whole slope was established on the satellite map, and the optimal route was planned according to the storage memory of the camera and the battery capacity of the UAV. After the UAV completed aerial photography along the designed route, the corresponding elevation points were established. Finally, the real 3D surface of the slope and the contour map of the slope in CAD were obtained according to the processing of relevant software. The real 3D surface of the slope is shown in Fig. 9 a, and the contour map of the slope in CAD is shown in Fig. 9 b.

The terrain generator function in Midas was applied to the scanning results to construct the real terrain surface of the slope. The slope's 1:1 3D model was generated through the entity expansion function. Figure 10 a shows the 3D slope model is shown in Fig. 10 a. The actual rock strata distribution of the slope was obtained using the borehole imaging technique. The slope was mainly categorized into sandstone, slate, and limestone. Rock strata were divided based on the borehole television results, as shown in Fig. 10b.
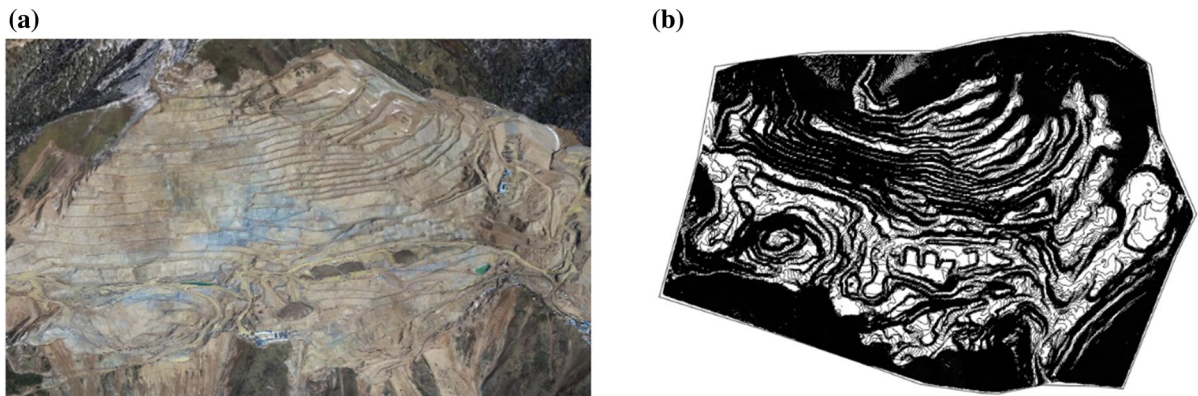
(a)

(b)

Fig. 9 UAV scanning results: **a** Real 3D surface of the slope; **b** Contour map of the slope in CAD

6.2 Determination of Rock Strata Parameters and Grid Division

The actual mechanical parameters of rock mass depend on the strength of rock blocks (obtained from laboratory tests) and the influence of actual structural planes (such as cracks and occurrence). To validate the numerical calculation results, more accurate rock mass parameters were obtained. The actual rock mass parameters were estimated using borehole imaging technology, a GSI system, and the Hoek–Brown strength criterion. The specific methods were obtained from the literature (Wu et al. 2018; Zhang 2008). The Hoek–Brown constitutive model was used in this simulation. The results of the rock laboratory test are shown in Table 6, and the estimated values of rock mass are shown in Table 7.

In Table 6, σ_{ci} is the uniaxial compressive strength of the intact rock, and E is the elastic modulus.

In Table 7, σ'_{cm}, c', and , ϕ' were the estimated values of uniaxial compressive strength, cohesion, and internal friction angle of the actual rock mass (considering the influence of the structural plane), respectively.

Tables 6 and 7 present the rock mass parameters used in the numerical calculation. A tetrahedral mesh was used to grid the 3D slope model; the partition results are shown in Fig. 10c.

6.3 Boundary Conditions and Mining Settings

In the simulation of the blasting vibration conditions, gravity load was first applied in the negative direction of the Z axis. Automatic constraints were added around the slope. A viscous boundary was adopted, making the boundary of the model meet the absorption condition of incident wave when it accepts dynamic load. The damping coefficient was 0.157. The recorded particle vibration time history curve (taking the curve 50 m in D4 as an example) at the blasting vibration monitoring site A was inputted, and observation points B′, C′, and D′ were set behind at
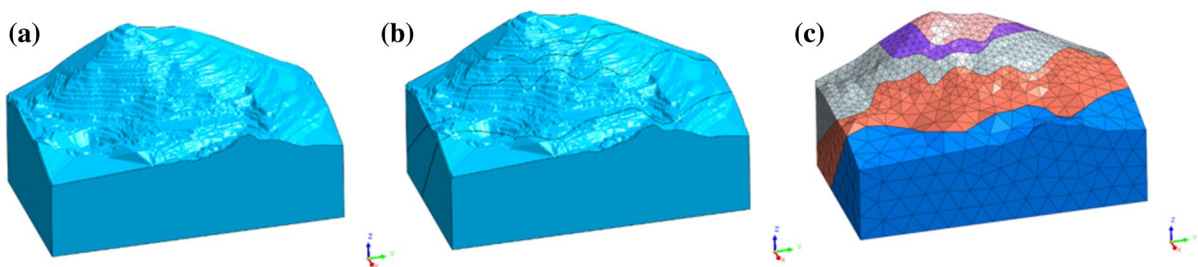
(a) **(b)** **(c)**

Fig. 10 3D model of the slope: **a** Before the strata were divided; **b** After the strata were divided; **c** Meshing of the model

Table 6 Rock laboratory test results

Rock types	Indicators				
	Bulk density	Porosity	Poisson's ratio	σ_{ci}/(MPa)	E/(GPa)
Sandstone	24.1	5.6	0.25	97.2	27.1
Slate	25.2	1.5	0.21	153.7	43.3
Limestone	24.9	1.4	0.21	112.5	51.5

Table 7 Hoek–Brown estimation results of rock mass strength

Rock types	Indicators		
	$\sigma'cm$/(MPa)	c'/(MPa)	ϕ'/(°)
Sandstone	3.35	0.95	25.54
Slate	9.95	1.66	39.05
Limestone	5.66	1.29	32.68

10 m, 20 m, and 30 m, respectively, to record their vibration velocities. The entire process was a transient calculation, from receiving the vibration signal to the end, and the duration was approximately 0.5 s. The peak particle vibration velocity was approximately 0.2 s, and an output was obtained every 0.1 s (Hou et al. 2015).

6.4 Numerical Calculation Results

In the initial state, that is, when no vibration signal was received, the slope was only subjected to gravity load. The calculation results are shown in Fig. 11.

The initial state calculation results showed that the minimum displacement along the X direction in the positive direction was approximately 0.0014 m, and the maximum displacement was approximately 0.0639 m; the western slope displacement was larger. The results are shown in Fig. 11 a. The displacement of the western slope was mainly along the negative direction of the Y direction while its maximum value was approximately 0.0315 m. The displacement of the eastern slope was mainly along the positive Y direction while its maximum value was approximately 0.00227 m. The overall displacement of the western slope was larger. These results are shown in Fig. 11 b. Figure 11 c illustrates the slope displacements along the negative Z direction where the displacement at the top of the western slope was larger; the maximum displacement was approximately 0.0418 m, and the minimum displacement was approximately 0.00166 m. As illustrated in Fig. 11 d, the potential

sliding surface range of the slope was in the western slope, and the safety factor of the slope was 1.195.

The numerical calculation results of the slope near the peak of blasting vibration velocity (0.2 s after receiving vibration signals) are shown in Fig. 12.

The calculation results of the slope stability 0.2 s after the start of the blasting vibration showed that the minimum displacement along the X direction was approximately 0.00101 m, the maximum displacement was approximately 0.0816 m, and the western slope displacement was larger; the maximum displacement along the X direction increased by 0.0177 m relative to the initial state. These results are shown in Fig. 12 a. The displacement of the western slope was mainly along the negative Y direction while its maximum value was approximately 0.0399 m; the displacement of the eastern slope was along the positive Y direction while its maximum value was approximately 0.00231 m; the overall displacement of the western slope was larger. These results are shown in Fig. 12 b. The maximum displacement in the negative direction of the western slope increased by 0.0085 m relative to the initial state, whereas the maximum displacement in the positive eastern slope Y direction increased by 0.00004 m. For the slope displacements along the negative Z direction, the displacement at the top of the western slope was larger, the maximum displacement was approximately 0.0482 m, and the minimum displacement was approximately 0.00129 m; the maximum displacement in the negative Y direction increased by 0.0065 m relative to the initial state, as shown in Fig. 12 c. As shown in Fig. 12 d, the potential sliding surface range of the slope remained in the western slope, and the safety factor of the slope was 1.170 0.2 s after blasting vibration started.

The numerical calculation results showed that the potential sliding surface range of the slope was in the western slope. The angle of the western slope was larger than that of the eastern slope, which is similar to real conditions. Moreover, small pieces of rubble fall in the western slope occasionally; hence, support
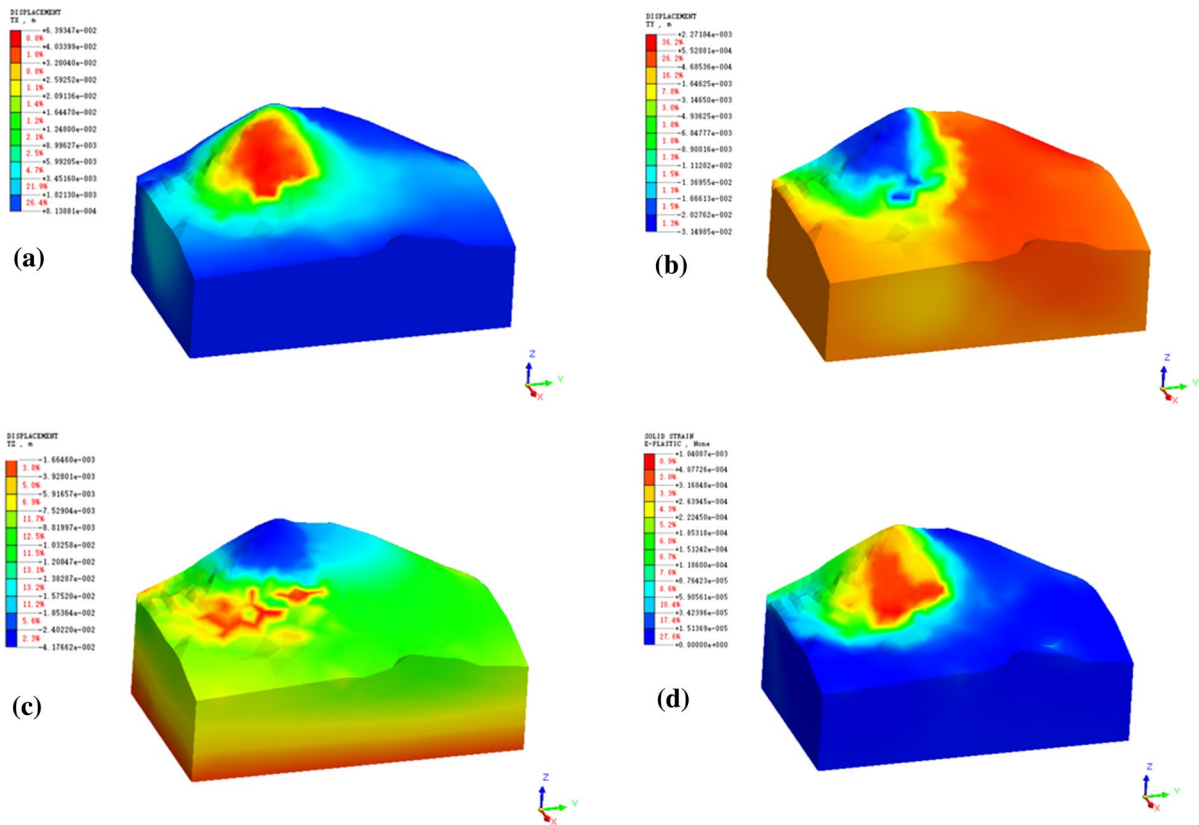
Fig. 11 Calculation results of the initial state: **a** Contour map of displacement in the X direction; **b** Contour map of displacement in the Y direction; **c** Contour map of displacement in the Z direction; **d** Contour map of effective plastic strain

measures should be strengthened for the western slope.

The output safety factor is illustrated in Table 8.

After the blasting vibration, the counter of the calculation and safety coefficient of slope was restored to the initial state. It was observed that under safe blasting conditions, the safety coefficient in the vibration time was reduced in low amplitude but recoverable after the vibration; moreover, the blasting activitiesdid not cause considerable damage to the slope. These observations further confirm that the blasting activities of the slope were in the safe range.

The fitting curve of the peak vibration velocity recorded at observation points B′, C′, and D′ as well as the vibration attenuation law described above are shown in Fig. 13.

Figure 13 shows the fitting curve of the peak vibration velocity recorded at observation points B′,C′, and D′; the figure also illustrates the vibration attenuation law described above.

Figure 13 demonstrates that the peak vibration velocity of observation points B′,C′ and D′ in the numerical calculation was consistent with the vibration attenuation law curve fitted by the previously measured points, indicating that the numerical calculation results were accurate.

7 Conclusion

We monitored the blasting vibration and measured the acoustic velocity of the slope of an open-pit gold mine in Manaoke, and we performed numerical calculations of the blasting vibration conditions using Midas. The following conclusions were drawn from the study:

(1) The fitting formula of the vibration attenuation law of the slope was obtained through blasting vibration monitoring and regression analysis, and
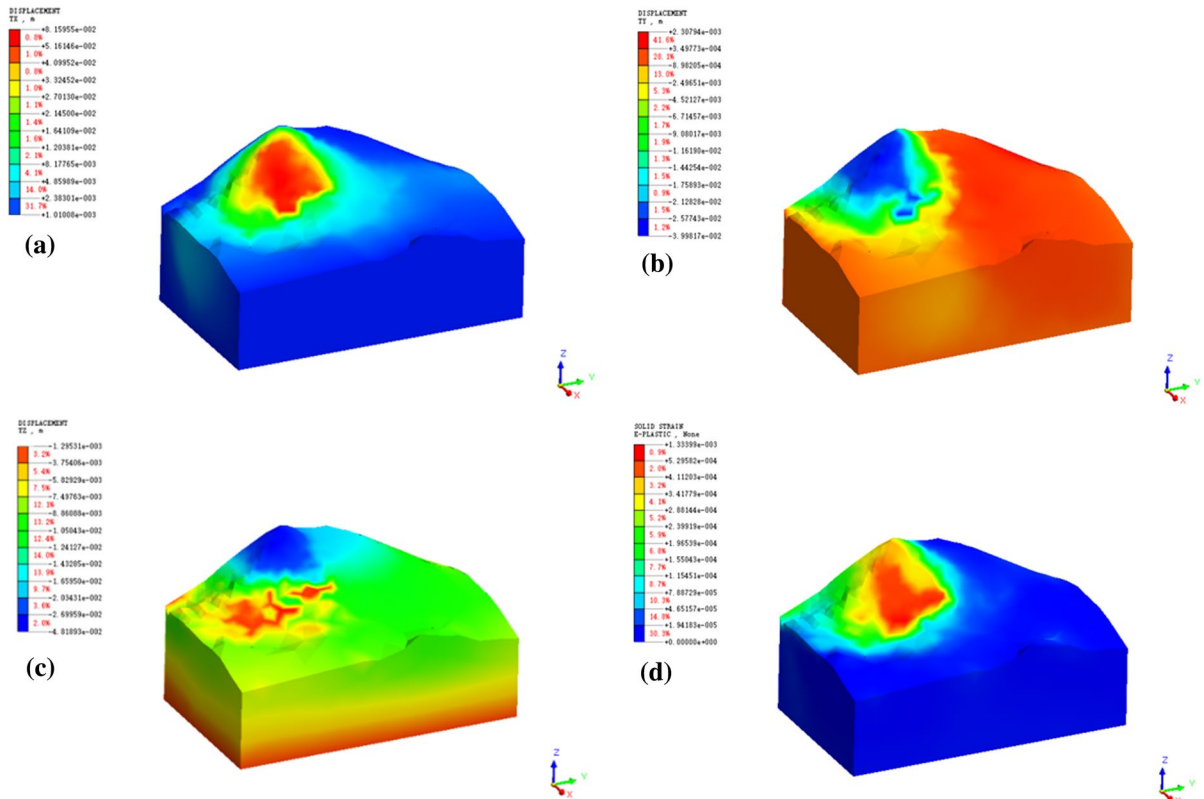
Fig. 12 Calculation results near vibration peak: **a** Contour map of displacement in the X direction; **b** Contour map of displacement in the Y direction; **c** Contour map of displacement in the Z direction; **d** Contour map of effective plastic strain

Table 8 Calculation results of safety factor

Time (s)	Safety factor
0 (initial state)	1.195
0.1	1.185
0.2 (peak of vibration)	1.170
0.3	1.190
0.4	1.190
0.5 (end of vibration)	1.195

the results showed that the blasting activity of the slope was in a safe range.

(2) Through acoustic velocity measurement and damage assessment, the damage depth of reserved rock mass under the current blasting conditions was 1.0–1.5 m.

(3) The least-square method was used to obtain the fitting curve between the damage depth of the reserved rock mass and the peak particle vibra-
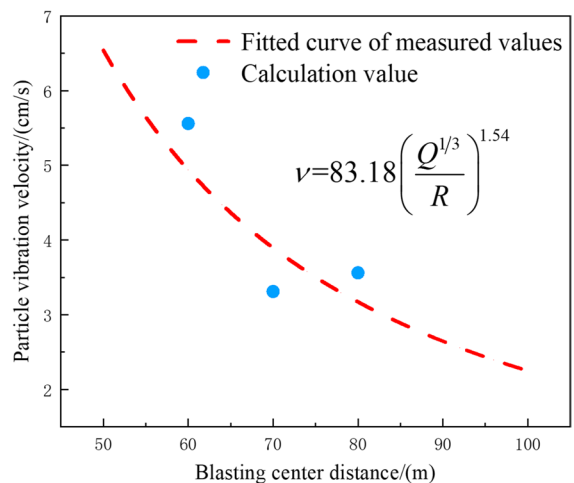

$$v = 83.18 \left(\frac{Q^{1/3}}{R} \right)^{1.54}$$

Fig. 13 Numerical calculation results of peak vibration velocity at different observation points

tion velocity at different blasting center distances. The damage depth of the reserved rock mass and the peak particle vibration velocity exhibited a good correlation. This finding can provide a method for predicting the future damage depth of reserved rock mass while serving as a reference for timely slope support construction.

(4) Unmanned aerial vehicle scanning technology can be used to obtain the real terrain surface of a slope efficiently, thereby providing a more convenient 3D modeling method for numerical calculations related to slopes.

(5) The numerical calculation results from the Midas software showed that the slope was in a stable state with a safety factor of 1.195. The potential sliding surface was on the western slope; hence, local monitoring measures should be strengthened in time. When the vibration velocity peaked, the impact on the western slope surface was more obvious, and the safety factor reduced to 1.170. However, after the vibration, the safety factor was restored to the initial state, indicating that the current production blasting activities were within a safe range. The fitting curve of the peak vibration velocity of the observation point was consistent with that of the measured point, demonstrating the accuracy of the numerical calculation results.

References

Ak H, Konuk A (2008) The effect of discontinuity frequency on ground vibrations produced from bench blasting: a case study. Soil Dyn Earthq Eng 28(9):686–694

Aloui M, Abbes C (2019) Fracturing influence on the propagation of the blast-induced ground vibrations: a case study. Geotech Geol Eng 37(6): 5327–5339

He L, Wang J, Xiao J, Tang L, Lin Y (2013) Pre-splitting blasting vibration reduction effect research on weak rock mass. Disaster Adv 6(3):338–343

Hou TS, Wang XG, Pamukcu S (2015) Geological characteristics and stability evaluation of wanjia middle school slope in wenchuan earthquake area. Geotech Geol Eng 34(1):1–13

Lu W, Zhou Z, Liu T, Liu Y (2012) Discrete element simulation analysis of rock slope stability based on Udec. Adv Build Mater Struct Eng 461:384

Mesec J, Kovac I, Soldo B (2010) Estimation of particle velocity based on blast event measurements at different rock units. Soil Dyn Earthq Eng 30(10):1004–1009

Man K, Liu X, Song Z (2021) Blasting vibration monitoring scheme and its application. J Vibroeng 23(7):1640–1651

Nateghi R (2012) Evaluation of blast induced ground vibration for minimizing negative effects on surrounding structures. Soil Dyn Earthq Eng 43:133–138

Niu J, Jiang X, Wang F (2018) Stability analysis of rock slope with small spacing tunnel under earthquakes and influence of ground motion parameters. Geotech Geol Eng 36(4):2437–2453

Peng YX, Wu L, Su Y, Chen CH (2016) Study on the effect of elevation on the prediction of underwater drill and blasting vibration frequency. Geosyst Eng 19(4):170–176

Rao ZB, Cai SJ (2016) The blasting test and blasting vibration monitoring of vertical crater retreat mining method in the luohe iron mine. Geotech Geol Eng 34(4):1047–1056

Roy N, Sarkar R (2017) A review of seismic damage of mountain tunnels and probable failure mechanisms. Geotech Geol Eng 35(1):1–28

Song GM, Shi XZ, Zhou ZG, Chen SR, Xiao QH (2000) Monitoring and Assessing Method for Blasting Vibration On Open-Pit Slope in Hainan Iron Mine. J Cent South Univ T 7(2):72–74

Shen H, Klapperich H, Abbas SM, Ibrahim A (2012) Slope stability analysis based on the integration of Gis and numerical simulation. Automat Constr 26:46–53

Wei XY, Zhao ZY, Gu J (2009) Numerical simulations of rock mass damage induced by underground explosion. Int J Rock Mech Min 46(7):1206–1213

Wu S, Jiang R, Zhang S, Zhang M (2018) Application of a modified hoek-brown strength criterion to borehole stability analysis. Rock Soil Mech 392:1–13

Wang Z, Gu W, Liang T, Zhao S, Chen P, Yu L (2020) Monitoring and prediction of the vibration intensity of seismic waves induced in underwater rock by underwater drilling and blasting. Def Technol 18(1):109–118

Xie LL, Lu WB, Gu JC, Wang GH (2018) Excavation method of reducing blasting vibration in complicated geological conditions. Shock Vib 2018:2518209

Yan C (2007) Blasting cumulative damage effects of underground engineering rock mass based on sonic wave measurement. J Cent South Univ T 14(2):230–235

Zhang LA (2008) Generalized three-dimensional hoek-brown strength criterion. Rock Mech Rock Eng 41(6):893–915

Zhu M, Wei PG, Zhang JG, Si XD (2019) Automatic monitoring system of blasting vibration and its application based on Tc6850. Information Technology In Geo Engineering: 25 September 2019, 336–352